



# Synthesis of zeolite UZM-35 and catalytic properties of copper-exchanged UZM-35 for ammonia selective catalytic reduction

Jeong Hwan Lee<sup>a,1</sup>, Young Jin Kim<sup>a,1</sup>, Taekyung Ryu<sup>a</sup>, Pyung Soon Kim<sup>b</sup>, Chang Hwan Kim<sup>b</sup>, Suk Bong Hong<sup>a,\*</sup>

<sup>a</sup> Center for Ordered Nanoporous Materials Synthesis, School of Environmental Science and Engineering, POSTECH, Pohang 790-784, Republic of Korea

<sup>b</sup> Advanced Catalysts and Emission-Control Research Lab, Research & Development Division, Hyundai Motor Group, Hwaseong 445-706, Republic of Korea

## ARTICLE INFO

### Article history:

Received 11 June 2016

Received in revised form 19 July 2016

Accepted 20 July 2016

Available online 20 July 2016

### Keywords:

UZM-35 and Cu-UZM-35

Synthesis

Characterization

NH<sub>3</sub>-SCR

Hydrothermal stability

## ABSTRACT

The synthesis of zeolite UZM-35 with the MSE topology and the catalytic properties of copper-exchanged UZM-35 (Cu-UZM-35) for the selective catalytic reduction of NO<sub>x</sub> with NH<sub>3</sub> (NH<sub>3</sub>-SCR) are presented. When the simple dimethyldipropylammonium cation is used as an organic structure-directing agent together with Na<sup>+</sup> and K<sup>+</sup>, crystallization of pure UZM-35 is very sensitive not only to the types of Al and Si sources employed, but also to the SiO<sub>2</sub>/Al<sub>2</sub>O<sub>3</sub> and K<sub>2</sub>O/(Na<sub>2</sub>O + K<sub>2</sub>O) ratios in the synthesis mixture. In the temperature range studied, fresh Cu-UZM-35 shows comparable deNOx performance to fresh Cu-SSZ-13, the best NH<sub>3</sub>-SCR catalyst known to date. When hydrothermally aged at 750 °C, although the latter catalyst outperforms the former one, the operating temperature window of Cu-UZM-35 is considerably wider than that of Cu-SSZ-13. Like Cu-beta, Cu-UZM-35 also produces a higher amount of N<sub>2</sub>O during SCR than Cu-SSZ-13 and Cu-ZSM-5. However, it shows a significantly lower NH<sub>3</sub> oxidation activity than Cu-SSZ-13 and Cu-ZSM-5. The overall characterization results of this study demonstrate the highly stable nature of framework Al atoms in the large-pore zeolite UZM-35 and their strong interactions with Cu<sup>2+</sup> ions. This may lead to a moderate alteration of exchanged Cu<sup>2+</sup> ions to CuO<sub>x</sub> and CuAl<sub>2</sub>O<sub>4</sub> phases at high temperatures, thus rendering Cu-UZM-35 hydrothermally stable during NH<sub>3</sub>-SCR.

© 2016 Elsevier B.V. All rights reserved.

## 1. Introduction

Nitrogen oxides (NO<sub>x</sub>) are the major source of acid rain and photochemical smog, continuously threatening the health of mankind [1]. With the popularization of high fuel-efficient diesel vehicles, their emission has become a primary environmental concern. Consequently, ever-tightening emission standards have been issued worldwide to improve air quality [2]. Among the deNOx technologies currently available, selective catalytic reduction of NO<sub>x</sub> with urea (urea-SCR) is recognized as the most effective and promising technology to meet the strict upcoming emission regulations such as Euro VI and EPA Tier 3 [3,4].

In general, the diesel exhaust temperature ranges from 150 to 350 °C. Hence, much attention has been focused on transition metal-exchanged zeolites with an excellent low-temperature SCR activity, primarily copper-exchanged ZSM-5 (framework type MFI) with two intersecting 10-ring channels [5,6]. However, their low

hydrothermal stability has placed an obstacle in the way of commercial success, because the diesel exhaust temperature can rise periodically to above 700 °C during the regeneration of diesel particulate filters installed before or after the SCR reactor [7,8]. In this regard, the discovery by BASF researchers in 2009 [9] that especially after being hydrothermally aged at 750 °C, Cu-SSZ-13 (CHA) with large 20-hedral ([4<sup>12</sup>6<sup>2</sup>8<sup>6</sup>]) cha-cages connected by small 8-ring windows, becomes much more active for reducing NO<sub>x</sub> than Cu-ZSM-5, the best low-temperature NH<sub>3</sub>-SCR catalyst up to that time [10,11], offered a major breakthrough in the urea-SCR technology. Since then, considerable efforts have been devoted not only to the elucidation of the nature of active sites in Cu-SSZ-13 [12–15], but also to the search for other copper-exchanged zeolites that could be hydrothermally more stable during NH<sub>3</sub>-SCR than Cu-SSZ-13.

Zeolite MCM-68 (MSE) was first discovered in 1997 by Weston and Dhingra of Mobil, with the patent being released a few years later [16]. As shown in Fig. 1, MCM-68 contains a three-dimensional pore system consisting of one type of straight 12-ring (6.4 × 6.8 Å) channels and two types of tortuous 10-ring (5.2 × 5.8 and 5.2 × 5.2 Å) channels. The two 10-ring channels intersect with each other, forming a large cylindrical cage circumscribed by 12-

\* Corresponding author.

E-mail address: [sbHong@postech.ac.kr](mailto:sbHong@postech.ac.kr) (S.B. Hong).

<sup>1</sup> These authors contributed equally.

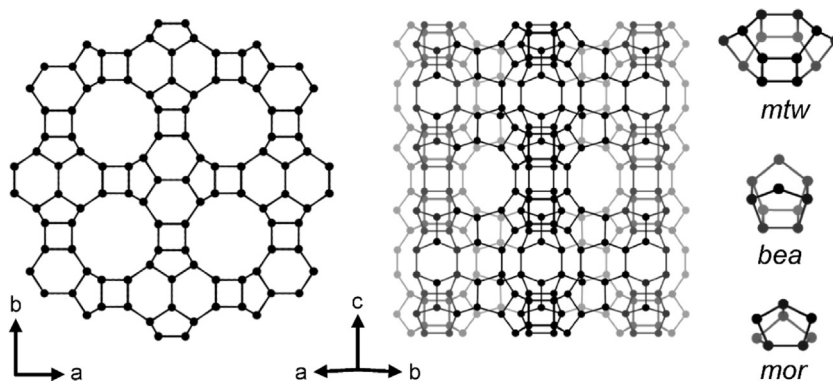


**Fig. 1.** MSE structure and its composite building units.

and 18-rings, with four 10-ring windows into the 12-ring straight channels [17,18]. Such unique structural features have allowed this large-pore zeolite to show interesting catalytic properties for various hydrocarbon conversions [19–23]. It is interesting to note here that the composite building units (i.e., *mor*, *bea*, and *mtw*) found in MCM-68 are exactly the same as those in the large-pore zeolite beta (\*BEA) [18] which is known as one of stable zeolite supports for transition metal-based deNOx catalysts [11,24]. To our knowledge, however, no studies have addressed the adequacy of MCM-68 as a support for any deNOx catalyst. MCM-68 was originally synthesized from a potassium aluminosilicate gel using the complicated and thus expensive cation *N,N,N,N'*-tetraethylbicyclo[2.2.2]oct-7-ene-2,3:5,6-dipyrrolidinium (TEBOP<sup>2+</sup>) as an organic structure-directing agent (SDA). Hence, there is a drive to find simpler organic SDAs that can give this zeolite to facilitate its industrial application.

UZM-35 is an MSE-type zeolite crystallized from sodium-potassium aluminosilicate gels in the presence of dimethyldipropylammonium (DMDPA<sup>+</sup>) ions [25], much simpler and cheaper than the already known organic SDAs leading to the synthesis of MCM-68. However, there is little known on the crystallization conditions and the composition of synthesis mixtures required for UZM-35 formation [25]. Here we describe our attempts to synthesize pure UZM-35 by varying the types of both Al and Si sources and the SiO<sub>2</sub>/Al<sub>2</sub>O<sub>3</sub> and K<sub>2</sub>O/(Na<sub>2</sub>O+K<sub>2</sub>O) ratios in the synthesis mixture. We also report the catalytic properties of copper-exchanged UZM-35 (Cu-UZM-35) for NH<sub>3</sub>-SCR. The catalytic results are compared with those of Cu-beta, as well as of Cu-SSZ-13 and Cu-ZSM-5, the two most widely studied catalysts for this reaction. Changes in the physicochemical properties of Cu-UZM-35 caused by hydrothermal aging at high temperatures have been characterized by using <sup>27</sup>Al MAS NMR, NH<sub>3</sub> temperature-programmed desorption, H<sub>2</sub> temperature-programmed reduction, UV-vis, X-ray photoelectron, and Cu K-edge X-ray absorption near edge structure spectroscopies.

## 2. Experimental

### 2.1. Zeolite synthesis

The reagents employed included dimethyldipropylammonium hydroxide (DMDPAOH, 40%, Sachem), aluminum hydroxide (Al(OH)<sub>3</sub>·1.0H<sub>2</sub>O, Aldrich), aluminum isopropoxide (Al[OCH(CH<sub>3</sub>)<sub>2</sub>]<sub>3</sub>, 98%, Aldrich), aluminum metal (99.5%, Wako), pseudobohemite (Al<sub>2</sub>O<sub>3</sub>·0.7H<sub>2</sub>O, Capatal B, Vista), aluminum nitrate (Al(NO<sub>3</sub>)<sub>3</sub>·9H<sub>2</sub>O, 98%, Junsei), colloidal silica (Ludox HS-40, Dupont), fumed silica (Aerosil 200, Degussa), and tetraethylorthosilicate (98%, Aldrich). KOH (45% aqueous solution, Aldrich) and NaOH (50% aqueous solution, Aldrich) were also used for zeolite synthesis. The Si source was first mixed with a solution of Al source and DMDPAOH in water. Then, an aqueous

solution of KOH and NaOH was added to this mixture. The final composition of typical synthesis mixtures used here was 4.5DMDPAOH·xK<sub>2</sub>O·(1-x)Na<sub>2</sub>O·yAl<sub>2</sub>O<sub>3</sub>·10SiO<sub>2</sub>·150H<sub>2</sub>O, where x and y are varied between 0 ≤ x ≤ 1 and 0 ≤ y ≤ 1, respectively. After being stirred at a room temperature for 2 h, the synthesis mixture was loaded into Teflon-lined 45 mL autoclave and heated at 175 °C for 7–14 days under static conditions. The solid products were recovered by filtration or centrifugation, washed repeatedly with distilled water, and dried overnight.

As-made UZM-35 was calcined in air at 550 °C for 8 h to remove the occluded organic SDA. The calcined zeolite was then refluxed twice in 1.0 M NH<sub>4</sub>NO<sub>3</sub> (2.0 g solid per 100 mL solution) for 6 h followed by calcination at 550 °C for 8 h in order to ensure that the zeolite was completely in its proton form. For comparison, SSZ-13 (Si/Al = 14) was synthesized by the inter-zeolite conversion of high-silica USY (Si/Al = 15, CBV720, Zeolyst) [14], and ZSM-5 (Si/Al = 14, HSZ-830NHA) and beta (Si/Al = 13, CBV814E) were purchased from Tosoh and Zeolyst, respectively. The Cu<sup>2+</sup>-exchanged form of all zeolite catalysts employed here were prepared by ion exchange of the ammonium form of the corresponding zeolites three times with 0.01 M Cu(CH<sub>3</sub>COO)<sub>2</sub> (97%, Aldrich) solutions at room temperature for 6 h followed by drying at 110 °C for 12 h and calcination at 500 °C for 5 h [14]. To investigate their hydrothermal stabilities, these Cu<sup>2+</sup> ion-exchanged zeolites were aged under flowing air containing 10% H<sub>2</sub>O at 650, 750, and 850 °C for 24 h.

### 2.2. Catalysis

The deNO<sub>x</sub> activity tests were conducted under atmospheric pressure in a fixed-bed flow reactor (3/8-in.-od Al tube) [3]. Prior to each experiment, 0.6 g of catalyst in the 20/30 mesh size packed in the reactor system were pretreated from room temperature to 500 °C at a ramp rate of 10 °C min<sup>-1</sup> under air flow (2000 mL min<sup>-1</sup>) and kept at the final temperature for 2 h. A feed gas stream consisting of 500 ppm NH<sub>3</sub>, 500 ppm NO, 5% O<sub>2</sub>, 10% H<sub>2</sub>O, and N<sub>2</sub> balance was then supplied, and the catalytic activity was measured at a gas hourly space velocity (GHSV) of 100,000 h<sup>-1</sup> under the steady-state conditions at each reaction temperature (150–500 °C). The inlet and outlet concentrations of NO were determined online by a Thermo Nicolet 6700 FT-IR spectrometer equipped with a 2 m gas cell. NH<sub>3</sub> oxidation was conducted under the identical reaction conditions described above except that the NO feed was stopped.

### 2.3. Analytical methods

Powder X-ray diffraction (XRD) patterns were measured on a PANalytical X'Pert diffractometer (Cu K $\alpha$  radiation) with an X'Celerator detector. Elemental analyses for Si, Al, and Cu were carried out by a Jarrell-Ash Polyscan 61E inductively coupled plasma

spectrometer in combination with a Perkin-Elmer 5000 atomic absorption spectrophotometer. The C, H, and N contents of the samples were analyzed by using a Vario EL III elemental organic analyzer. Thermogravimetric analyses were performed on an SII EXSTAR6000 thermal analyzer, where the weight loss related to the desorption of water was further confirmed by differential thermal analyses using the same analyzer. Crystal morphology and average size were determined by Hitachi S4800 scanning electron microscope (SEM). N<sub>2</sub> sorption experiments were performed on a Mirae SI nanoPorosity-XG analyzer.

NH<sub>3</sub> temperature-programmed desorption (TPD) was recorded on a fixed bed, flow-type apparatus linked to a Hewlett-Packard 5890 series II gas chromatograph with a thermal conductivity detector. 0.1 g of sample were activated in flowing He (50 mL min<sup>-1</sup>) at 550 °C for 2 h. Then, 10 wt% NH<sub>3</sub> was passed over the sample at 150 °C for 0.5 h. The treated sample was subsequently purged with He at the same temperature for 1 h to remove physisorbed NH<sub>3</sub>. TPD was performed in flowing He (30 mL min<sup>-1</sup>) from 150 to 700 °C with a heating rate of 10 °C min<sup>-1</sup>. H<sub>2</sub> temperature-programmed reduction (TPR) was measured on a Micromeritics AutoChem II 2920 analyzer. The sample pretreated at 500 °C for 1 h with 5% O<sub>2</sub> in Ar flow was cooled to room temperature, and then heated to 800 °C at a heating rate of 10 °C min<sup>-1</sup> with 5% H<sub>2</sub> in Ar flow. The IR spectra of pyridine molecules chemisorbed on the proton form of zeolites employed here were measured on a Nicolet 6700 FT-IR spectrometer using self-supporting zeolite wafers of ca. 13 mg cm<sup>-2</sup> activated under vacuum at 500 °C for 2 h in a home-made IR cell with CaF<sub>2</sub> windows. After contacting with pyridine vapor (6.0 × 10<sup>2</sup> Pa) at 100 °C for 0.5 h in the IR cell followed by desorption (10<sup>-1</sup> Pa) at 300 °C for 2 h, the concentrations of Brønsted and Lewis acid sites in zeolites were determined from the intensities of the IR bands by using the integrated area of a given band with the molar extinction coefficient given in the literature [26].

The solution <sup>13</sup>C NMR spectra were recorded in 5 mm quartz tubes on a Bruker AVANCE III 300 spectrometer at a <sup>13</sup>C frequency of 75.475 MHz with a π/2 rad pulse length of 10.2 μs and a recycle delay of 1.5 s. Multinuclear MAS NMR measurements were performed on a Varian Inova 300 spectrometer at a spinning rate of 6.0 kHz. The <sup>1</sup>H-<sup>13</sup>C CP MAS spectra were measured at a <sup>13</sup>C frequency of 75.43 MHz with a π/2 rad pulse length of 7.0 μs, a recycle delay of 240 s, and an acquisition of ca. 1000 pulse transients. The <sup>29</sup>Si MAS spectra were recorded at a <sup>29</sup>Si frequency of 59.590 MHz with a π/2 rad pulse length of 5.0 μs, recycle delay of 30 s, and an

acquisition of 1000–2500 pulse transients. The <sup>13</sup>C and <sup>29</sup>Si chemical shifts are reported relative to TMS. The <sup>27</sup>Al MAS NMR were measured at a <sup>27</sup>Al frequency of 78.156 MHz using a pulse length of 1.8 μs and a recycle delay of 0.5 s. Approximately 3000 pulse transients were accumulated, and the <sup>27</sup>Al chemical shifts are reported relative to an Al(H<sub>2</sub>O)<sub>6</sub><sup>3+</sup> solution. To more clearly examine changes in the <sup>27</sup>Al resonance intensity caused by hydrothermal aging, the amount of copper-exchanged zeolites used in <sup>27</sup>Al MAS NMR measurements was kept exactly constant.

The UV-vis spectra were recorded on a Shimadzu UV-2501PC spectrometer in diffuse reflectance mode between 200 and 800 nm at a step of 0.5 nm with a slit width of 1.0 nm. BaSO<sub>4</sub> was used as a reference sample to determine the baseline spectrum. The X-ray photoelectron spectroscopy (XPS) analysis was performed on a ThermoK-Alpha spectrometer equipped with a Mg Kα X-ray source (1253.6 eV). All the binding energies are referenced to the C(1s) line of adventitious carbon at 284.6 eV. The X-ray absorption near edge structure (XANES) spectra at the Cu K-edge were collected on the 7D1 beamline at the Pohang Accelerator Laboratory (PAL) using a Si (111) crystal monochromator. Cu foil was employed for the energy calibration ( $E_0 = 8979.0$  eV). The X-ray intensity was monitored using ionization chambers purged with pure N<sub>2</sub> gas at room temperature for the incident ( $I_0$ ) and transmitted ( $I_t$ ) beam in the Cu K-edge measurements. Cu<sub>2</sub>O (≥99.99%, Aldrich), CuO (99.99%, Aldrich), and CuAl<sub>2</sub>O<sub>4</sub>, synthesized by a modification of the method reported by Luo et al. [27], were used as reference compounds. The distribution of Cu species in aged catalysts were semi-quantified by linear combination fits of XANES spectra using the IFEFFIT 1.2.11 freeware suite.

### 3. Results and discussion

**Table 1** lists the representative products obtained using DMDPAOH as an organic SDA and synthesis mixtures with different oxide compositions under the conditions described above. In each case, the products listed were the only ones obtained in repeated trials. Our initial attempts to synthesize UZM-35 were made to reproduce the reported synthesis under static conditions using an aluminosilicate gel with the oxide composition 4.0DMDPAOH·1.0K<sub>2</sub>O·1.0Na<sub>2</sub>O·0.5Al<sub>2</sub>O<sub>3</sub>·10SiO<sub>2</sub>·240H<sub>2</sub>O that was obtained by slightly modifying example 1 in the original UOP patent [25]. Here, we used aluminum hydroxide and colloidal silica as Al and Si sources, respectively. However, we always obtained a mix-

**Table 1**  
Syntheses from oxide composition 4.5DMDPAOH·xK<sub>2</sub>O·(1-x)Na<sub>2</sub>O·yAl<sub>2</sub>O<sub>3</sub>·10SiO<sub>2</sub>·150H<sub>2</sub>O.<sup>a</sup>

Al source <sup>b</sup>	Si source <sup>c</sup>	Gel composition		Product <sup>d</sup>	
		x	y	t = 7 days	t = 14 days
AH	CS	0	0.5	mordenite + UZM-35	mordenite + UZM-35
AH	CS	0.25	0.5	UZM-35+(ZSM-5)	UZM-35+ZSM-5
AH	CS	0.50	0.5	amorphous	UZM-35+offretite
AH	CS	0.75	0.5	UZM-35	UZM-35+offretite
AH	CS	1.00	0.5	UZM-35+offretite	UZM-35+offretite
AlP	CS	0.75	0.5	offretite + UZM-35	offretite + UZM-35
AM	CS	0.75	0.5	amorphous	offretite + UZM-35
PB	CS	0.75	0.5	amorphous +(ZSM-5)	UZM-35+mordenite
AN	CS	0.75	0.5	amorphous	ZSM-5+UZM-35
AH	FS	0.75	0.5	amorphous + ZSM-5	ZSM-5+UZM-35
AH	TEOS	0.75	0.5	ZSM-5 + amorphous	ZSM-5+UZM-35
AH	CS	0.75	1.0	amorphous	amorphous
AH	CS	0.75	0.25	ZSM-5	ZSM-5
AH	CS	0.75	0.1	ZSM-5	ZSM-5
AH	CS	0.75	0	ZSM-5	ZSM-5

<sup>a</sup> All syntheses were carried out under static condition at 175 °C.

<sup>b</sup> AH, aluminum hydroxide; AlP, aluminum isopropoxide; AM, aluminum metal; PB, pseudobohemite; AN, aluminum nitrate.

<sup>c</sup> CS, colloidal silica (Ludox HS-40); FS, fumed silica (Aerosil 200); TEOS, tetraethylorthosilicate.

<sup>d</sup> The product appearing first is the major phase, and the product obtained in a trace amount is given in parentheses.

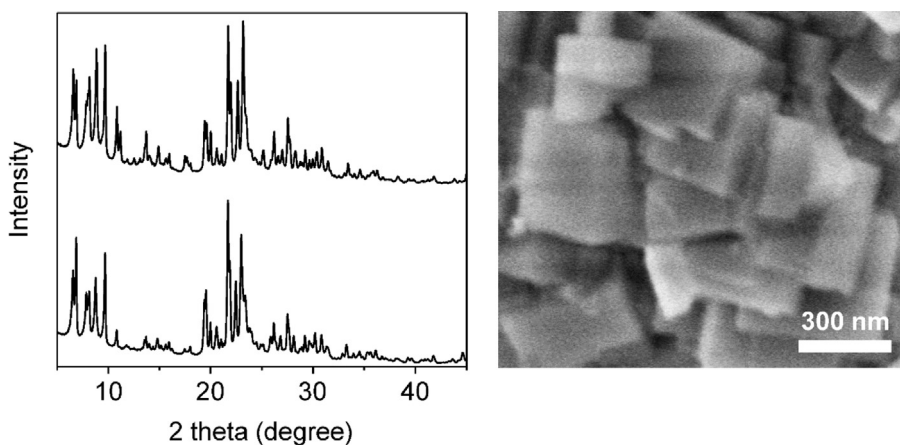


**Fig. 2.** Powder XRD patterns (left) of the as-made (bottom) and proton (top) forms of UZM-35 and SEM image (right) of as-made UZM-35.

ture of UZM-35 and offretite (OFF), where the former zeolite was the major phase, after heating at 175 °C for 7 days. To crystallize UZM-35 in its pure form, therefore, we adjusted for various synthesis parameters including K<sub>2</sub>O/(K<sub>2</sub>O + Na<sub>2</sub>O), DMDPAOH/SiO<sub>2</sub>, and H<sub>2</sub>O/SiO<sub>2</sub> ratios, while keeping the SiO<sub>2</sub>/Al<sub>2</sub>O<sub>3</sub> ratio constant. As a result, we were able to synthesize pure UZM-35 by heating an aluminosilicate gel with the composition 4.5DMDPAOH-0.75K<sub>2</sub>O-0.25Na<sub>2</sub>O-0.5Al<sub>2</sub>O<sub>3</sub>-10SiO<sub>2</sub>-150H<sub>2</sub>O at 175 °C for 7 days (Table 1). It thus appears that UZM-35 crystallization is highly sensitive to the K<sub>2</sub>O/(K<sub>2</sub>O + Na<sub>2</sub>O) ratio in the synthesis mixture. This is different from the synthesis of MCM-68 in which K<sup>+</sup> is the only inorganic SDA required [21]. However, UZM-35 was not so stable in the synthesis conditions, because additional 7 days of heating in the crystallization medium gave offretite as an impurity.

Table 1 also shows that the types of both Al and Si sources employed are another important factor affecting the phase purity of this large-pore zeolite. While the replacement of aluminum hydroxide with the equivalent amount of aluminum isopropoxide, aluminum metal, pseudobohemite, or aluminum nitrate under the conditions where the crystallization of UZM-35 proved to be reproducible yielded offretite, mordenite (MOR), or ZSM-5 as an impurity, the use of fumed silica or tetraethylorthosilicate instead of colloidal silica always gave ZSM-5, together with a considerable amount of amorphous phase or UZM-35. When the K<sub>2</sub>O/(K<sub>2</sub>O + Na<sub>2</sub>O) ratio in the aluminosilicate gel was fixed to 0.75, on the other hand, a decrease in SiO<sub>2</sub>/Al<sub>2</sub>O<sub>3</sub> ratio to 10 gave no crystalline phases. However, ZSM-5 was the phase that crystallized from synthesis mixtures with SiO<sub>2</sub>/Al<sub>2</sub>O<sub>3</sub> ratios >20. Such a high dependence on the SiO<sub>2</sub>/Al<sub>2</sub>O<sub>3</sub> ratio was also observed for the TEBOP<sup>2+</sup>-mediated synthesis of MCM-68 [21].

Fig. 2 shows the powder XRD patterns of the as-made and proton forms of UZM-35 synthesized in this work. Comparison with the literature data reveals that both forms are highly crystalline and no reflections other than those from the MSE structure are observed [18]. The SEM photograph shows that this zeolite appears as rectangular cuboids of ca. 300 nm in length and ca. 150 nm in height (Fig. 2) that are somewhat larger than MCM-68 with a crystal size of <100 nm in length [28]. A combination of elemental and thermal analyses indicates that as-made UZM-35 has a unit cell composition of |K<sub>3.7</sub>Na<sub>0.4</sub>DMDPA<sub>7.2</sub>(H<sub>2</sub>O)<sub>13.1</sub>||Al<sub>11.3</sub>Si<sub>100.7</sub>O<sub>224</sub>|. Thus, no noticeable enrichment of Al in the product (SiO<sub>2</sub>/Al<sub>2</sub>O<sub>3</sub> = 18) with respect to the synthesis mixture (SiO<sub>2</sub>/Al<sub>2</sub>O<sub>3</sub> = 20) was found. However, a negligible amount of Na<sup>+</sup> present suggests that under the synthesis conditions studied here, the structure-directing role of K<sup>+</sup> in UZM-35 formation is considerably stronger than that of Na<sup>+</sup>, although

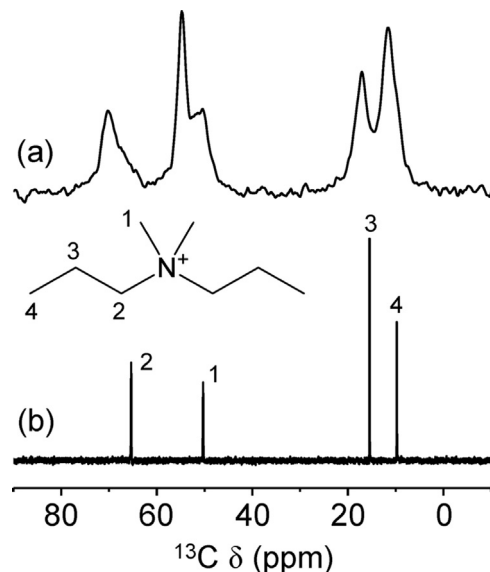


**Fig. 3.** <sup>13</sup>C NMR spectra of organic SDA, DMDPA<sup>+</sup>, showing the assignment of each resonance: (a) <sup>1</sup>H-<sup>13</sup>C CP MAS NMR spectra of as-made UZM-35 with DMDPA<sup>+</sup> occluded in the pores and (b) <sup>13</sup>C NMR of DMDPAOH in D<sub>2</sub>O solution.

the absence of the latter cation in the synthesis mixture yielded mordenite as a major phase (Table 1).

Fig. 3 compares the <sup>1</sup>H-<sup>13</sup>C CP MAS NMR spectrum of as-made UZM-35 with the solution <sup>13</sup>C NMR spectrum of DMDPAOH. The resonance of the methyl carbons of organic species in as-made UZM-35 splits into two peaks at 55 and 50 ppm, unlike that of the corresponding carbon atoms of free DMDPA<sup>+</sup>. This indicates that two different degrees of geometric constraints and van der Waals interactions with the zeolite framework are imposed on the methyl groups of the encapsulated DMDPA<sup>+</sup> cations, while the organic SDAs remain intact upon their occlusion into the UZM-35 pores. A similar conclusion can also be observed for the case of the methylene carbons bonded to the nitrogen atom of the occluded organic SDA molecules.

The <sup>27</sup>Al and <sup>29</sup>Si MAS NMR spectra of the as-made and proton forms of UZM-35 can be found in Supplementary Fig. S1. The <sup>27</sup>Al MAS NMR spectra of both materials are characterized by only one sharp resonance around 55 ppm, typical of tetrahedral Al in the zeolite framework. The lack of noticeable resonances corresponding to octahedral Al in the <sup>27</sup>Al MAS NMR spectrum of H-UZM-35 suggests the remarkable thermal stability of this large-pore zeolite, despite its relatively high Al content (SiO<sub>2</sub>/Al<sub>2</sub>O<sub>3</sub> = 18). However,

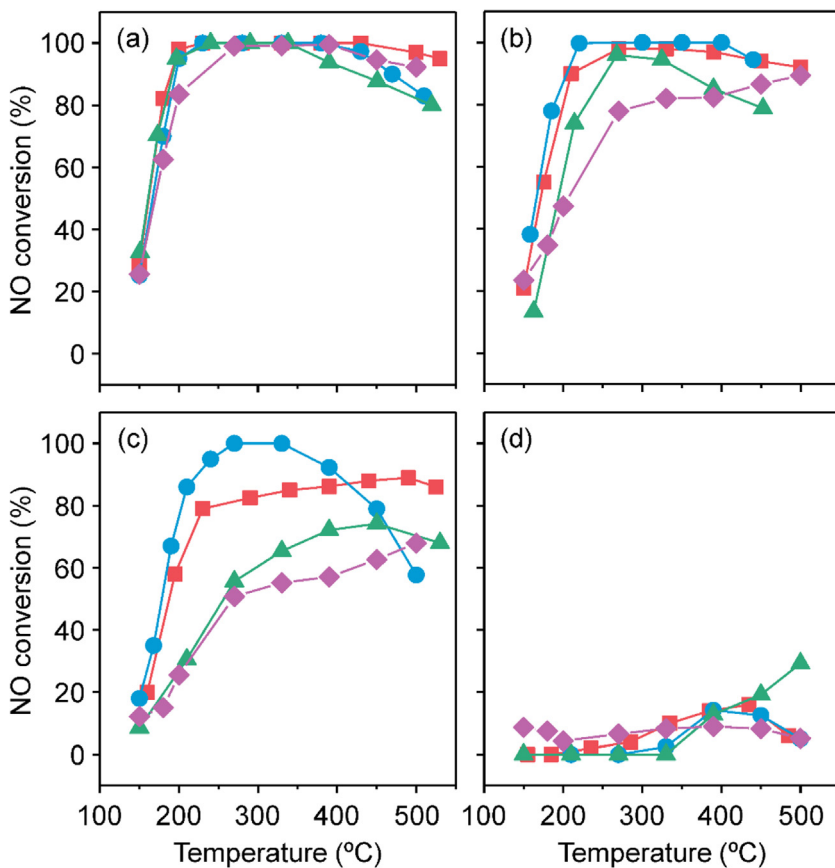


**Fig. 4.** NO conversion as a function of temperature in  $\text{NH}_3$ -SCR reaction over (a) fresh, (b) 650 °C-, (c) 750 °C-, and (d) 850 °C-aged Cu-UZM-35 (■), Cu-SSZ-13 (●), Cu-ZSM-5 (▲), and Cu-beta (◆) catalysts. The feed contains 500 ppm  $\text{NH}_3$ , 500 ppm NO, 5%  $\text{O}_2$ , and 10%  $\text{H}_2\text{O}$  balanced with  $\text{N}_2$  at 100,000  $\text{h}^{-1}$  GHSV. Hydrothermal aging was performed under flowing air containing 10%  $\text{H}_2\text{O}$  at the desired temperature for 24 h.

the presence of a weak band at  $3665 \text{ cm}^{-1}$  due to OH groups belonging to extraframework Al in its IR spectrum (Supplementary Fig. S2) indicates that partial dealumination has occurred during the organic SDA removal and successive  $\text{NH}_4^+$  ion exchange recalcination steps. This can be further supported by some differences in the line shape between the  $^{29}\text{Si}$  MAS NMR spectra of the as-made and proton forms of UZM-35.

Fig. 4 shows NO conversion as a function of temperature in  $\text{NH}_3$ -SCR reaction over the Cu-UZM-35, Cu-SSZ-13, Cu-ZSM-5, and Cu-beta hydrothermally aged at 650, 750, and 850 °C, respectively, as well as over their fresh form, which were measured at 500 ppm  $\text{NH}_3$ , 500 ppm NO, 5%  $\text{O}_2$ , 10%  $\text{H}_2\text{O}$ , and 100,000  $\text{h}^{-1}$  GHSV in the feed. Since their Cu contents ( $3.1 \pm 0.2 \text{ wt\%}$ ) are similar to one another (Table 2), the catalytic data in Fig. 4 could illustrate the effects of the framework structure of zeolite supports. It can be seen that the low-temperature deNOx activity of fresh Cu-UZM-35 is slightly better than that of fresh Cu-beta but is comparable to the activities of fresh Cu-SSZ-13 and Cu-ZSM-5 [5,6,9]. Fig. 4 also shows that Cu-UZM-35 and Cu-beta containing 12-ring channels gave higher NO conversion at  $\geq 450^\circ\text{C}$  than Cu-SSZ-13 and Cu-ZSM-5.

There are no beneficial effects on the deNOx activity of fresh Cu-UZM-35 in both low- and high-temperature regions (Supplementary Fig. S3), although its Cu content increased from 3.3 to 4.3 wt% ( $\text{Cu}/\text{Al} = 0.50$ ). It thus appears that the aggregation and/or sintering of Cu species in this large-pore zeolites may be easier at a higher Cu content [14]. On the other hand, the  $\text{NH}_3$  oxidation activities of Cu-UZM-35 and Cu-beta were found to be fairly lower than those of the other two catalysts (Supplementary Fig. S4). This suggests that the  $\text{NH}_3$  consumption efficiency at elevated

temperatures during SCR can differ according to the structure type of zeolite supports. However, the consumption efficiency of  $\text{Cu}^{2+}$ -exchanged zeolite catalysts may not always be higher in large-pore zeolite supports than in small-pore ones, because the  $\text{NH}_3$  oxidation activities of  $\text{Cu}^{2+}$  ion exchanged into the high-silica ( $\text{Si}/\text{Al} \geq 11$ ) LTA-type zeolites with a cage-based small-pore structure are even lower than the activity of Cu-UZM-35 [29], unlike the oxidation activity of Cu-SSZ-13.

When hydrothermally aged at 650 °C for 24 h, Cu-UZM-35 exhibited marginally lower NO conversion than Cu-SSZ-13 in the temperature range studied here. As shown in Fig. 4, however, hydrothermal aging at 750 °C led to larger differences in the low-temperature deNOx activity. Although the NO conversion (ca. 65%) at 200 °C of aged Cu-UZM-35 is fairly lower than the conversion (ca. 80%) of aged Cu-SSZ-13, for example, the opposite holds for comparison with the values (ca. 30 and 25%, respectively) of aged Cu-ZSM-5 and Cu-beta. Of particular interest is that the operating temperature window aged Cu-UZM-35 is considerably wider than that of any of the other three catalysts. The formation of  $\text{N}_2\text{O}$ , an undesired by-product, in  $\text{NH}_3$ -SCR reaction over the four different  $\text{Cu}^{2+}$ -exchanged zeolites before and after hydrothermal aging at 750 °C is compared in Fig. 5. While high selectivity to  $\text{N}_2$  with little amount of  $\text{N}_2\text{O}$  was observed over Cu-SSZ-13 and Cu-ZSM-5 even after hydrothermal aging [11,14], a higher amount of  $\text{N}_2\text{O}$  was observed for Cu-UZM-35, as well as for Cu-beta [11], than for the former two catalysts. This suggests that the extent of  $\text{N}_2\text{O}$  formation over the  $\text{Cu}^{2+}$  ions exchanged into zeolites, which is a result of the decomposition of  $\text{NH}_4\text{NO}_3$  formed during SCR, is greatly affected by the type of zeolite support structures [30]. However, the details are beyond the scope of this work.

**Table 2**

Physicochemical properties of copper-exchanged zeolite catalysts studied in this work.

Catalyst	Zeolite pore topology	Cu <sup>a</sup> (wt%)	Si/Al <sup>a</sup>	Cu/Al <sup>a</sup>	N <sub>2</sub> BET surface area <sup>b</sup> (m <sup>2</sup> g <sup>-1</sup> )		Acidity <sup>c</sup> (μmol pyridine g <sup>-1</sup> )	
					Fresh	Aged at 750 °C	Brønsted	Lewis
Cu-UZM-35	3D, 12 and 10-ring channel system	3.3	8.9	0.38	460	370	154	38
Cu-SSZ-13	3D, cage system with 8-ring windows	2.9	14	0.49	560	450	— <sup>d</sup>	— <sup>d</sup>
Cu-ZSM-5	3D, 10-ring channel system	3.0	14	0.50	360	300	158	17
Cu-beta	3D, 12-ring channel system	3.1	13	0.45	570	200	116	59

<sup>a</sup> Determined by elemental analysis.

<sup>b</sup> Calculated from N<sub>2</sub> adsorption data.

<sup>c</sup> Determined from the intensities of the IR bands of retained pyridine at 1545 and 1455 cm<sup>-1</sup> after desorption at 300 °C for 2 h, respectively, by using the extinction coefficients given by Emeis [26].

<sup>d</sup> Not determined due to the considerably small dimension (3.8 × 3.8 Å) of its 8-ring cage windows compared with the kinetic diameter (5.7 Å) of pyridine.

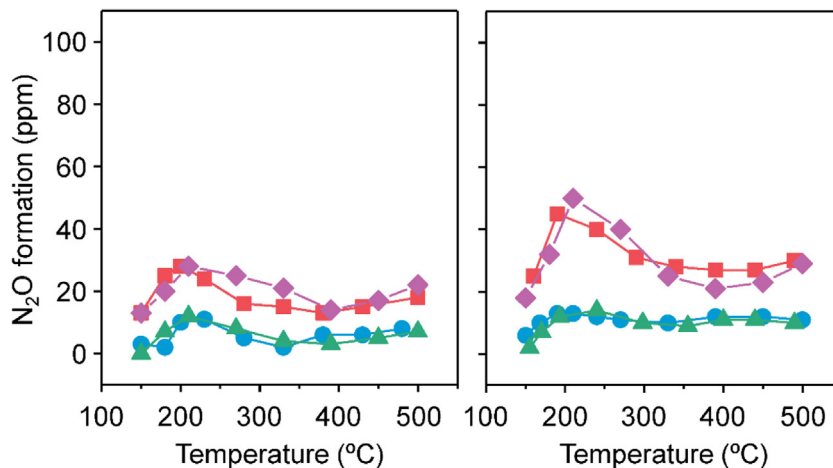


**Fig. 5.** N<sub>2</sub>O formation as a function of temperature in NH<sub>3</sub>-SCR reaction over Cu-UZM-35 (■), Cu-SSZ-13 (●), Cu-ZSM-5 (▲), and Cu-beta (◆) before (left) and after (right) hydrothermal aging. The feed composition and hydrothermal aging conditions at 750 °C are the same as those in Fig. 4.

The powder XRD patterns of aged Cu-UZM-35, Cu-SSZ-13, and Cu-ZSM-5 at 750 °C reveal that the majority of their frameworks remains intact, which is not the case of Cu-beta (Supplementary Fig. S5). N<sub>2</sub> sorption measurements show that the BET surface areas of the former three catalysts are smaller by ca. 20% than the values of their fresh form, respectively (Table 2). Therefore, notable differences in their deNOx performance caused by hydrothermal aging at 750 °C should be attributed to differences in the composition and chemical state of supported copper species rather than to those in the extent of structural collapse of the zeolite support. However, the surface area of aged Cu-beta is only one third of the value of fresh Cu-beta, indicating that its poor deNOx performance may be mainly due to the hydrothermal instability of zeolite beta at 750 °C. When hydrothermally aged at 850 °C, on the other hand, all Cu<sup>2+</sup> ion-exchanged zeolites have lost their structural integrity practically, explaining their poor deNOx activities (Fig. 4). Because differences in the NH<sub>3</sub>-SCR activity are largest upon hydrothermal aging at 750 °C, we have mainly characterized the physicochemical properties of the catalysts treated at this temperature, together with those of fresh catalysts. For convenience's sake, we will refer to the catalysts aged hydrothermally at 750 °C simply as aged catalysts from now on.

The effect of hydrothermal aging on the structure of zeolite supports was further investigated by <sup>27</sup>Al MAS NMR spectroscopy. As given in Supplementary Fig. S6, the <sup>27</sup>Al MAS NMR spectra of both fresh and aged forms of Cu-UZM-35, Cu-SSZ-13, Cu-ZSM-5, and Cu-beta show one resonance at 54–58 ppm, typical of tetrahedral Al in the zeolite framework. However, the intensity of the tetrahedral Al resonance was found to be fairly weaker in the spectra of each of the hydrothermally aged form. This implies that a non-negligible

portion of Al has been extracted from the zeolite framework during the hydrothermal aging step. As repeatedly reported [31,32], in addition, the lack of any octahedral Al resonance in Supplementary Fig. S6, can be attributed to the formation of CuAl<sub>2</sub>O<sub>4</sub> by reaction of paramagnetic Cu centers with extraframework Al species during hydrothermal aging [11]. Experimental evidence to support this speculation will be given below.

Fig. 6 shows the NH<sub>3</sub> TPD profiles from H-UZM-35, H-SSZ-13, H-ZSM-5, and H-beta. All the TPD profiles except the profile from H-beta are characterized by two desorption peaks with maxima in the temperature regions 250–270 and 430–510 °C which can be assigned to NH<sub>3</sub> desorption from weak and strong acid sites, respectively. No NH<sub>3</sub> desorption peaks at temperatures higher than 400 °C are detectable in the profile from H-beta, suggesting the very low concentration of strong acid sites in this large-pore zeolite. Interestingly, not only the total areas of NH<sub>3</sub> desorption but also the temperature maxima of low- and high-temperature desorption peaks are nearly the same for H-UZM-35 and H-ZSM-5. This suggests that the concentration and strength of both weak and strong acid sites in these two zeolites are similar to each other, which can also be evidenced by IR spectroscopy with adsorbed pyridine (Table 2). As shown in Fig. 6, in contrast, the relative area ratio of the high-temperature NH<sub>3</sub> desorption peak to low-temperature one is higher for H-SSZ-13 than for H-UZM-35 and H-ZSM-5. Also, the high-temperature desorption peak from H-SSZ-13 is located at a higher temperature (maximum around 510 °C), indicating that the strong acid sites in SSZ-13 possess a higher strength than those in the other two zeolites.

Fig. 6 also shows the NH<sub>3</sub> TPD profiles from Cu-UZM-35, Cu-SSZ-13, Cu-ZSM-5, and Cu-beta before and after hydrothermal

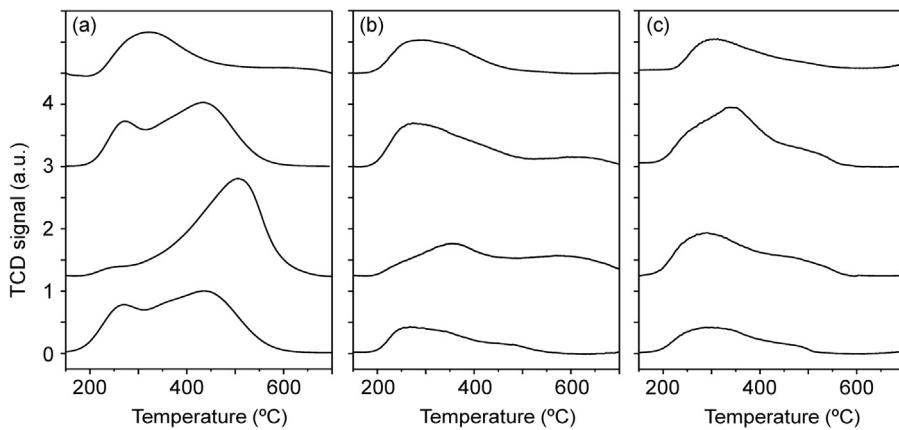


**Fig. 6.**  $\text{NH}_3$  TPD profiles of the (a) proton, (b)  $\text{Cu}^{2+}$ -exchanged, and (c)  $\text{Cu}^{2+}$ -exchanged, hydrothermally aged forms of (from bottom to top) UZM-35, SSZ-13, ZSM-5, and beta.

aging. When compared to their proton form, a much weaker high-temperature  $\text{NH}_3$  desorption peak is observed for the first three catalysts, regardless of aging treatment. This reveals that the strong acid sites in their proton form are mainly Brønsted acid sites. It is worth noting that fresh Cu-SSZ-13 gives a new broad desorption peak around  $350^\circ\text{C}$  that is not clearly visible not only in the TPD profiles from fresh Cu-UZM-35, Cu-ZSM-5, and Cu-beta, but also in the profile from H-SSZ-13. Therefore, we tentatively assign this peak to  $\text{NH}_3$  desorption from the  $\text{Cu}^{2+}$  ions in Cu-SSZ-13. While hydrothermal aging gave no significant changes in the profile from Cu-UZM-35 and Cu-beta, aged Cu-ZSM-5 exhibits a new desorption peak around  $340^\circ\text{C}$ . Because this peak is not well resolved in the profiles from aged Cu-SSZ-13 and Cu-UZM-35, which are still active for  $\text{NH}_3$ -SCR (Fig. 4), it appears to be due to  $\text{NH}_3$  desorption from the inactive Cu species in aged Cu-ZSM-5.

Fig. 7 shows the UV-vis spectra of fresh and aged Cu-UZM-35, Cu-SSZ-13, Cu-ZSM-5, and Cu-beta. The spectra of all fresh catalysts are characterized by two quite broad bands at  $<280$  and around  $780\text{ nm}$ , assignable to the  $\text{O} \rightarrow \text{Cu}^{2+}$  charge-transfer and the  $d-d$  transition of  $\text{Cu}^{2+}$  ( $3d^9$ ) ions, respectively [33–36], indicating the presence of isolated  $\text{Cu}^{2+}$  ions as a major Cu species in each catalyst [12,14]. Fig. 7 also shows that hydrothermal aging at  $750^\circ\text{C}$  yielded a red-shift of the charge-transfer band, probably due to the transformation of  $\text{Cu}^{2+}$  ions to oligonuclear  $[\text{Cu}-\text{O}-\text{Cu}]_n$  and/or crystalline  $\text{CuO}_x$  species [33–36]. Because the extent of band shift is higher in the order of Cu-SSZ-13 < Cu-beta ≈ Cu-UZM-35 < Cu-ZSM-5, sintering of Cu species appears to be severer on Cu-ZSM-5. Changes in the state of intrazeolitic  $\text{Cu}^{2+}$  ions during hydrothermal aging can also be reflected by differences in the intensity of the band around  $780\text{ nm}$  attributable to the  $d-d$  transition of  $\text{Cu}^{2+}$  ions. The fact that aged Cu-ZSM-5 gives a weaker  $d-d$  transition band than the corresponding form of the other three catalysts suggests the lower stability of  $\text{Cu}^{2+}$  ions exchanged into this medium-pore zeolite.

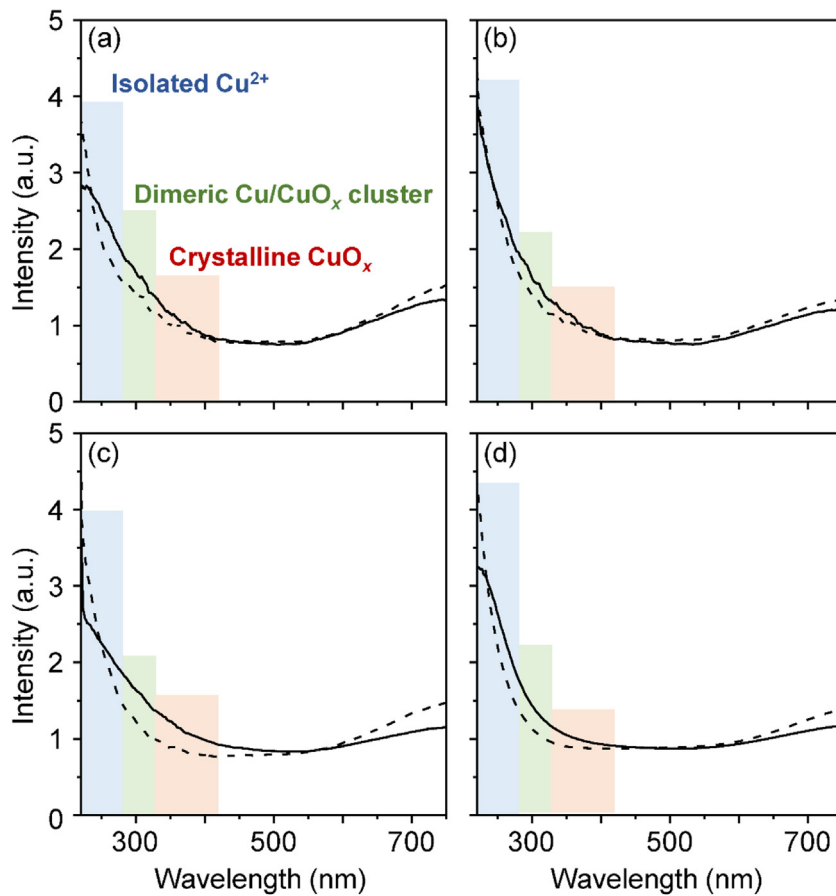
Fig. 8 compares the  $\text{H}_2$ -TPR profiles from fresh Cu-UZM-35, Cu-SSZ-13, and Cu-ZSM-5, and Cu-beta with those from aged corresponding catalysts. While all the fresh catalysts show a peak around  $200^\circ\text{C}$  due to the reduction of  $\text{Cu}^{2+}$  to  $\text{Cu}^+$  in the low temperature region, fresh Cu-UZM-35 gives an additional shoulder around  $260^\circ\text{C}$ , revealing the presence of more than one  $\text{Cu}^{2+}$  site in this large-pore zeolite [14,37]. We also note that the position of the reduction peak of  $\text{Cu}^+$  to  $\text{Cu}^0$  differs notably according to the type of zeolite support employed. For example, this reduction peak is observed around  $310^\circ\text{C}$  in the  $\text{H}_2$ -TPR profile from fresh Cu-ZSM-5. However, it appears around 510, 460, and  $450^\circ\text{C}$  in the profiles from fresh Cu-UZM-35, Cu-SSZ-13, and Cu-beta, respectively. These results indicate that the interaction of  $\text{Cu}^{2+}$  ions with the zeolite

framework are significantly weaker in Cu-ZSM-5 than in the other three catalysts [38]. Therefore, it appears that the exchanged  $\text{Cu}^{2+}$  ions are more easily changeable during hydrothermal aging in the former zeolite than in the latter three zeolites, which is consistent with the UV-vis results in Fig. 7.

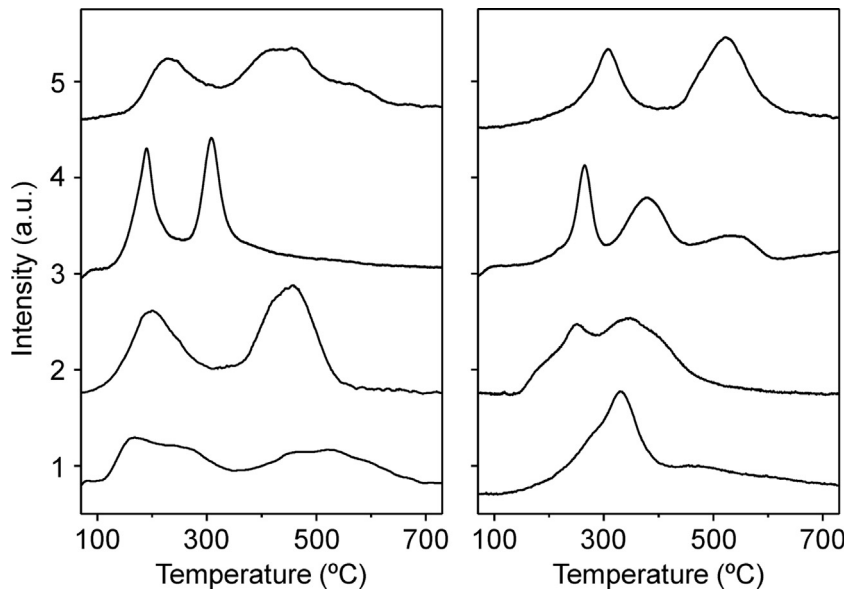
As repeatedly shown in previous studies [11,14], hydrothermal aging of Cu-ZSM-5 at  $750^\circ\text{C}$  resulted in the shift of the  $\text{Cu}^{2+}$  and  $\text{Cu}^+$  reduction peaks to the higher temperature region due to the migration of  $\text{Cu}^{2+}$  ions into the less reducible sites in ZSM-5 and/or to their transformation to  $\text{CuO}_x$ . Also, a new broad peak around  $530^\circ\text{C}$  assignable to the reduction of the inactive  $\text{CuAl}_2\text{O}_4$  phase for  $\text{NH}_3$ -SCR [11,27,39] is resolved in its  $\text{H}_2$ -TPR profile. Like the case of Cu-SSZ-13, however, the  $\text{H}_2$ -TPR results did not allow us to confirm the presence of the  $\text{CuAl}_2\text{O}_4$  phase in aged Cu-UZM-35 and Cu-beta. This is because their  $\text{Cu}^{2+}$  and  $\text{Cu}^+$  reduction peaks have shifted to the higher temperature region and could thus overlap with the  $\text{CuAl}_2\text{O}_4$  reduction peak.

Fig. 9 shows the  $\text{Cu}(2p_{3/2})$  XPS spectra of fresh and aged Cu-UZM-35, Cu-SSZ-13, Cu-ZSM-5, and Cu-beta. Three peaks at 932.7, 933.7, and 936.2 eV due to the  $\text{Cu}_2\text{O}/\text{Cu}^0$ ,  $\text{CuO}$ , and  $\text{Cu}(\text{OH})_2$ , respectively [40], are observable in the spectra of the four fresh catalysts. Also, there is a shake-up satellite peak around 945 eV, typical of  $\text{Cu}^{2+}$  due to the ligand to metal ( $\text{O}(2p) \rightarrow \text{Cu}(3d)$ ) electron transfer [41]. The formation of  $\text{Cu}_2\text{O}/\text{Cu}^0$  species on the surface of each catalyst is attributable to the reduction of  $\text{Cu}^{2+}$  ions by X-ray irradiation [42,43]. Since the isolated  $\text{Cu}^{2+}$  ions are the main Cu species in all fresh catalysts (Fig. 7), on the other hand, the  $\text{CuO}$  responsible for the peak at 933.7 eV should be assigned to the  $\text{Cu}^{2+}$  ions coordinated to the zeolite framework oxygen atoms [40]. Also, the presence of the  $\text{Cu}(\text{OH})_2$  peak indicates that the catalysts have not been fully dehydrated by evacuation at room temperature before XPS experiments. The relative distributions of Cu species present on the surface of zeolite catalysts employed here have been determined by deconvolution of the XPS spectra in Fig. 9 and are given in Table 3. It is clear that all four fresh catalysts possess  $\text{CuO}$  (i.e.,  $\text{Cu}^{2+}$  ions) as the primary surface copper species.

The deconvolution results in Fig. 9 and Table 3 also shows that a new  $\text{Cu}(2p_{3/2})$  XPS peak at 935.0 eV corresponding to  $\text{CuAl}_2\text{O}_4$  [41] becomes clearly visible after hydrothermal aging at  $750^\circ\text{C}$ . The formation of this compound can be further supported by an increase in intensity of the shake-up satellite peak around 945 eV, which is more apparent in the case of Cu-ZSM-5 and Cu-beta. The  $\text{CuAl}_2\text{O}_4$  phase with a partially inverse spinel structure where  $\text{Cu}^{2+}$  occupies the octahedral sites is known to show a stronger satellite peak [41,44]. The surface composition data in Table 3 reveal that the relative amounts of  $\text{CuAl}_2\text{O}_4$  in aged catalysts are higher in the order of Cu-SSZ-13 < Cu-UZM-35 < Cu-beta < Cu-ZSM-5.



**Fig. 7.** UV-vis spectra of (a) Cu-UZM-35, (b) Cu-SSZ-13, (c) Cu-ZSM-5, and (d) Cu-beta before (dotted line) and after (solid line) hydrothermal aging at 750 °C.



**Fig. 8.** H<sub>2</sub>-TPR profiles from (from bottom to top) Cu-UZM-35, Cu-SSZ-13, and Cu-ZSM-5, and Cu-beta before (left) and after (right) hydrothermal aging at 750 °C.

**Fig. 10** shows the Cu K-edge XANES spectra of Cu-UZM-35, Cu-SSZ-13, Cu-ZSM-5, and Cu-beta before and after hydrothermal aging at 750 °C. The typical characteristics of the Cu K-edge structure of octahedral Cu<sup>2+</sup> ions [7,14] are observed in the XANES spectra of the four fresh catalysts. However, aged catalysts exhibit two additional weak peaks around 8983 and 8985 eV which are assignable to the 1s → 4p electronic transition of Cu<sup>+</sup> and Cu<sup>2+</sup> ions,

respectively, both of which are coordinated to oxygen atoms, as confirmed by comparison with the spectra of pure Cu<sub>2</sub>O and CuO selected as reference compounds [12,14]. Also, there is a notable decrease in intensity of the white line appearing around 8995 eV, which is particularly true for both Cu-ZSM-5 and Cu-beta, revealing changes in the local environment of Cu atoms by a decrease in oxidation state of Cu species or sintering [45].

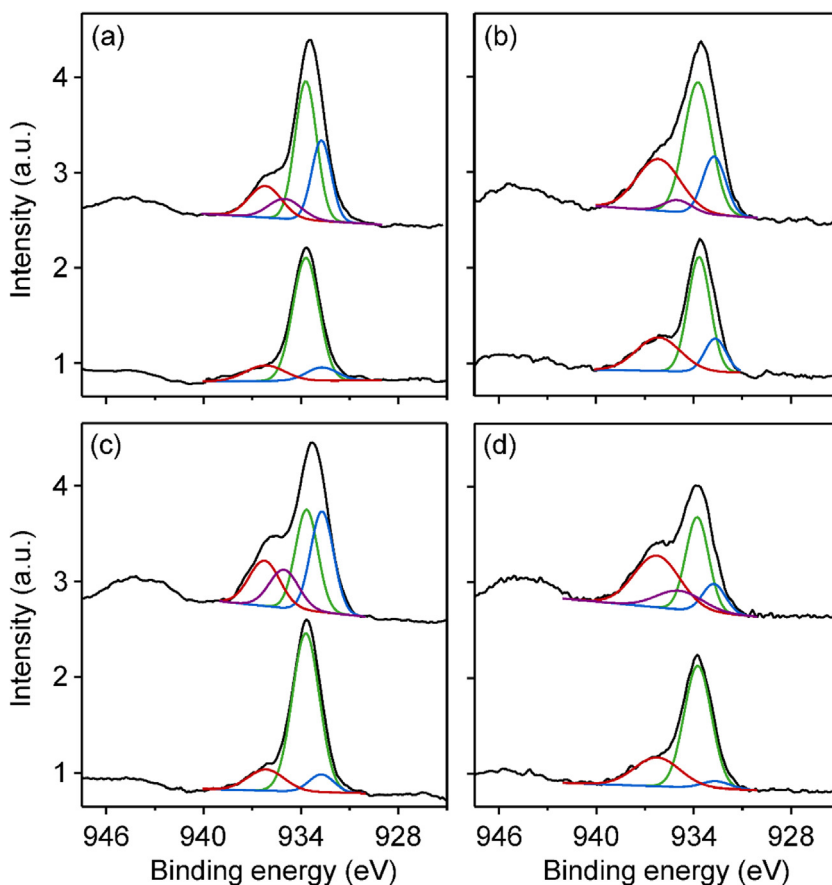


**Fig. 9.** Cu(2p<sub>3/2</sub>) XPS spectra of (a) Cu-UZM-35, (b) Cu-SSZ-13, (c) Cu-ZSM-5, and (d) Cu-beta before (bottom) and after (top) hydrothermal aging at 750 °C. The binding energy scale has been adjusted to C(1s) line at 284.6 eV. Cu<sub>2</sub>O/Cu<sup>0</sup>, blue; CuO, green; Cu(OH)<sub>2</sub>, red; CuAl<sub>2</sub>O<sub>4</sub>, purple (For interpretation of the references to colour in this figure legend, the reader is referred to the online version of this article.).

**Table 3**

Relative distributions of various copper species in Cu<sup>2+</sup>-exchanged zeolite catalysts with four different framework topologies.

Catalyst	Surface <sup>a</sup>				Bulk <sup>b</sup>			
	Cu <sub>2</sub> O/Cu <sup>0</sup> (%)	CuO (%)	Cu(OH) <sub>2</sub> (%)	CuAl <sub>2</sub> O <sub>4</sub> (%)	Cu <sup>2+</sup> (%)	Cu <sub>2</sub> O (%)	CuO (%)	CuAl <sub>2</sub> O <sub>4</sub> (%)
fresh Cu-UZM-35	9.8	75.8	14.4	–	81.1	–	18.9	–
fresh Cu-SSZ-13	14.9	54.2	30.9	–	88.6	–	11.4	–
fresh Cu-ZSM-5	7.8	78.5	13.7	–	88.5	–	11.5	–
fresh Cu-beta	4.1	68.9	27.0	–	79.7	–	20.3	–
aged Cu-UZM-35	25.3	47.8	16.5	10.4	49.7	9.1	35.4	5.8
aged Cu-SSZ-13	17.6	48.1	30.0	4.3	61.4	4.3	32.2	2.1
aged Cu-ZSM-5	32.5	32.0	19.7	15.8	32.5	27.2	29.7	10.6
aged Cu-beta	10.9	35.7	39.2	14.2	36.2	12.6	43.5	7.7

<sup>a</sup> Obtained by Cu(2p<sub>3/2</sub>) XPS analysis.

<sup>b</sup> Determined by K-edge XANES spectra using linear combination fitting.

To quantify the bulk distributions of various Cu species in all the catalysts before and after hydrothermal aging at 750 °C, we analyzed their XANES spectra using a linear combination fit of the spectra of reference compounds including CuO, Cu<sub>2</sub>O, and CuAl<sub>2</sub>O<sub>4</sub>. We also used fresh Cu-SSZ-13 with a low Cu content (0.91 wt%), which has been extensively studied in our recent work [14], as a reference for Cu<sup>2+</sup> ions. When fresh, Cu species exist predominantly as Cu<sup>2+</sup> ions with a minor fraction of CuO (Supplementary Table 3 and Fig. S7) which may be formed during the calcination step, in good agreement with the UV-vis and XPS results (Figs. 7 and 9, respectively). When aged, however, the distribution of Cu species differs notably according to the structure type of the zeolite support employed (Fig. 11 and Table 3). In particular, aged Cu-ZSM-5 has the largest amounts of Cu<sub>2</sub>O and CuAl<sub>2</sub>O<sub>4</sub> among all aged catalysts employed. Table 3 also shows that the relative portion of Cu<sup>2+</sup> ions

in aged catalysts is higher in the order of Cu-ZSM-5 < Cu-beta < Cu-UZM-35 < Cu-SSZ-13, which is slightly different from the order of their deNO<sub>x</sub> activities. As shown in Fig. 4, aged Cu-beta gives lower NO conversion at 250–450 °C than aged Cu-ZSM-5. This may in our view be attributed to the much higher degree of structural collapse of the zeolite support in the former catalyst, as clearly evidenced by a combination of powder XRD, <sup>27</sup>Al MAS NMR, and N<sub>2</sub> sorption results.

Given the lack of 8-rings in the large-pore zeolite UZM-35 and the overall results presented in this work, therefore, we conclude that the efficient zeolite supports for Cu<sup>2+</sup> ions do not necessarily belong to cage-based, small-pore materials such as SSZ-13 and SSZ-39 (AEI). The hydrothermal stability of copper-exchanged zeolites may in our view depend intrinsically on the framework topology of the zeolite support. The precise reason for the good

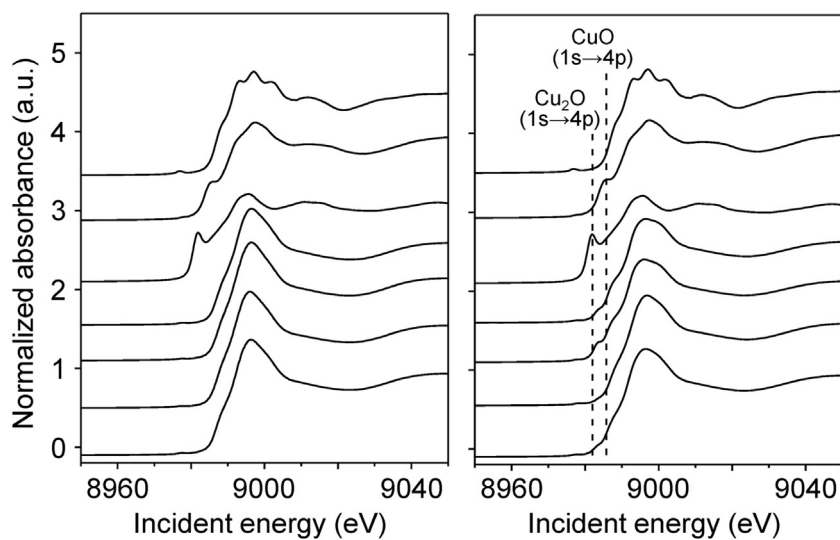


**Fig. 10.** Cu K-edge XANES spectra of (from bottom to top) Cu-UZM-35, Cu-SSZ-13, Cu-ZSM-5, Cu-beta, Cu<sub>2</sub>O, CuO, and CuAl<sub>2</sub>O<sub>4</sub> before (left) and after (right) hydrothermal aging at 750 °C.

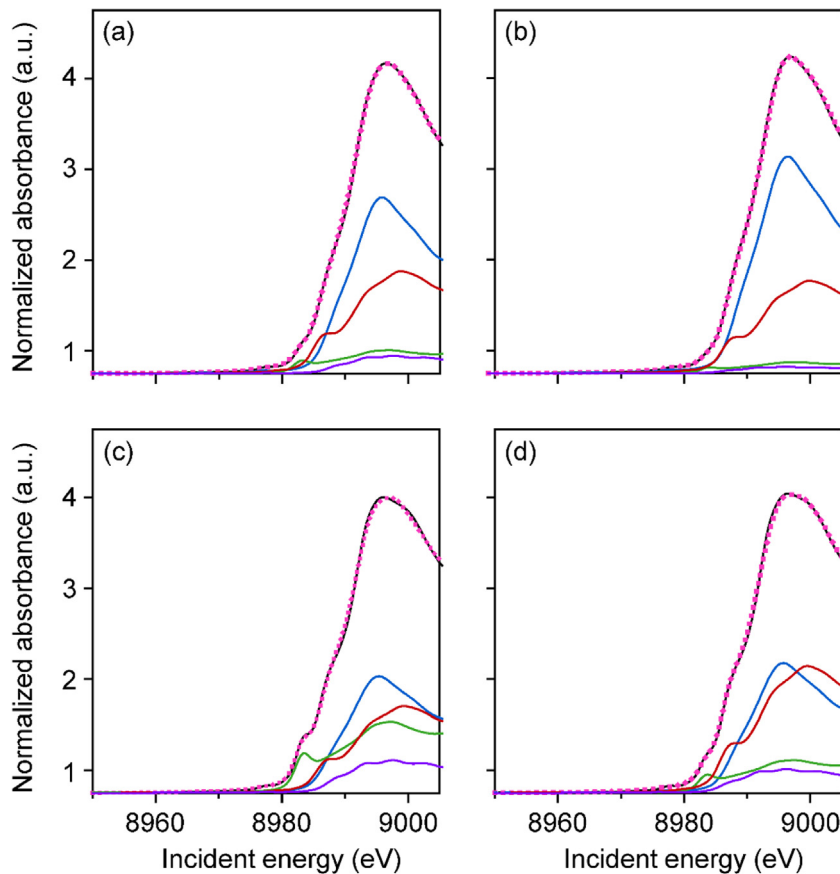


**Fig. 11.** Linear combination fits of the Cu K-edge XANES spectra of (a) Cu-UZM-35, (b) Cu-SSZ-13, (c) Cu-ZSM-5, and (d) Cu-beta catalysts aged hydrothermally at 750 °C. While the solid and dotted lines indicate the experimental data and linear combination fits, respectively, the blue, green, red, and purple solid lines represent the XANES spectra of Cu<sup>2+</sup>, Cu<sub>2</sub>O, CuO, and CuAl<sub>2</sub>O<sub>4</sub> references, respectively (For interpretation of the references to colour in this figure legend, the reader is referred to the online version of this article.).

hydrothermal stability of aged Cu-UZM-35 in NH<sub>3</sub>-SCR and thereby its wider operating temperature window than Cu-SSZ-13 is still unclear. However, it has been repeatedly shown that the Cu<sup>2+</sup> ions coordinated on the face of 8-hedral ([4<sup>6</sup>6<sup>2</sup>]) double 6-ring (*d*6*r*) units in Cu-SSZ-13 (CHA topology) are responsible for the excellent hydrothermal stability of this NH<sub>3</sub>-SCR catalyst [14,46,47].

As described above, UZM-35 with the MSE topology contains 8-hedral ([4<sup>2</sup>5<sup>4</sup>6<sup>2</sup>]) *mtw*, 4-hedral ([54]) *mor*, and 6-hedral ([4<sup>3</sup>5<sup>2</sup>6<sup>1</sup>]) *bea* as composite building units (CBUs). The 6-ring in *bea* CBUs is puckered-boat-shaped, but the same ring in *mtw* ones is much more flat. Moreover, the *mtw* CBUs possess 6-rings on both of their sides, like the *d*6*r*. If such is the case, the local environments of Cu<sup>2+</sup> ions

located near the *mtw* CBUs in Cu-UZM-35 could then be similar to those of the identical cations on the *d6r* units in Cu-SSZ-13, thus being hydrothermally stable. To check whether this speculation is correct, we are investigating the location and coordination of Cu<sup>2+</sup> ions in fresh Cu-UZM-35 using synchrotron powder XRD and Rietveld analyses.

#### 4. Conclusions

UZM-35 with the MSE topology was found to crystallize over a specific aluminosilicate composition in the presence of dimethylidipropylammonium, K<sup>+</sup>, and Na<sup>+</sup> ions as structure-directing agents. The synthesis of pure UZM-35 also requires the use of particular types of Al and Si sources (i.e., aluminum hydroxide and Ludox HS-40, respectively). While the NH<sub>3</sub>-SCR activity of fresh Cu-UZM-35 is slightly better than that of fresh Cu-beta, it is comparable to the activities of fresh Cu-SSZ-13 and Cu-ZSM-5 with similar Al and Cu contents. However, hydrothermal aging at 750 °C led to the low-temperature deNO<sub>x</sub> activity to be in the order of Cu-beta ≈ Cu-ZSM-5 < Cu-UZM-35 < Cu-SSZ-13. An unexpected finding is that the operating temperature window of aged Cu-UZM-35 is rather wider than that of aged Cu-SSZ-13, the best catalyst known for this reaction thus far. A combination of UV-vis, XPS, and XANES measurements demonstrate that the extent of transformation of exchanged Cu<sup>2+</sup> ions into CuO<sub>x</sub> and CuAl<sub>2</sub>O<sub>4</sub> phases during hydrothermal aging is higher in the order of Cu-SSZ-13 < Cu-UZM-35 < Cu-beta < Cu-ZSM-5. In contrast, the H<sub>2</sub>TPR results suggest that the interactions of Cu<sup>2+</sup> ions with the zeolite framework are considerably stronger in the first catalysts, rendering them hydrothermally more stable. Given the absence of 8-rings in the large-pore zeolite UZM-35 and the good hydrothermal stability of Cu-UZM-35, it is most likely that the efficient zeolite support for Cu<sup>2+</sup> ions as a NH<sub>3</sub>-SCR catalyst is not necessarily limited to small-pore materials with large cavities.

#### Acknowledgements

This work was supported by the National Creative Research Initiative Program (2012R1A3A2048833) through the National Research Foundation of Korea and by Hyundai Motor Group. We thank PAL for XANES beam time. PAL is supported by MSIP and POSTECH.

#### Appendix A. Supplementary data

Supplementary data associated with this article can be found, in the online version, at <http://dx.doi.org/10.1016/j.apcatb.2016.07.040>.

#### References

- [1] H. Bosch, F. Janssen, *Catal. Today* 2 (1988) 369.
- [2] W.S. Epling, L.E. Campbell, A. Yezers, N.W. Currier, J.E. Parks, *Catal. Rev.* 46 (2004) 163.
- [3] Y.J. Kim, H.J. Kwon, I. Heo, I.-S. Nam, B.K. Cho, J.W. Choung, M.-S. Cha, G.K. Yeo, *Appl. Catal. B* 126 (2012) 9.
- [4] M.V. Twigg, *Catal. Today* 163 (2011) 33.
- [5] J. Baik, S. Yim, I.-S. Nam, Y. Mok, J.-H. Lee, B. Cho, S. Oh, *Top. Catal.* 30 (2004) 37.
- [6] H. Sjövall, L. Olsson, E. Fridell, R.J. Blint, *Appl. Catal. B* 64 (2006) 180.
- [7] J.-H. Park, H.J. Park, J.H. Baik, I.-S. Nam, C.-H. Shin, J.-H. Lee, B.K. Cho, S.H. Oh, *J. Catal.* 240 (2006) 47.
- [8] K. Chen, K.S. Martirosyan, D. Luss, *Chem. Eng. Sci.* 66 (2011) 2968.
- [9] I. Bull, W.M. Xue, P. Burk, R.S. Boorse, W.M. Jaglowski, G.S. Kroemer, A. Moini, J.A. Patchett, J.C. Dettling, M.T. Caudle, US Patent 7,601,662 B2 (2009).
- [10] D.W. Fickel, E. D'Addio, J.A. Lauterbach, R.F. Lobo, *Appl. Catal. B* 102 (2011) 441.
- [11] J.H. Kwak, D. Tran, S.D. Burton, J. Szanyi, J.H. Lee, C.H.F. Peden, *J. Catal.* 287 (2012) 203.
- [12] U. Deka, A. Juhin, E.A. Eilertsen, H. Emerich, M.A. Green, S.T. Korhonen, B.M. Weckhuysen, A.M. Beale, *J. Phys. Chem. C* 116 (2012) 4809.
- [13] L. Wang, J.R. Gaudet, W. Li, D. Weng, *J. Catal.* 306 (2013) 68.
- [14] Y.J. Kim, J.K. Lee, K.M. Min, S.B. Hong, I.-S. Nam, B.K. Cho, *J. Catal.* 311 (2014) 447.
- [15] S.A. Bates, A.A. Verma, C. Paolucci, A.A. Parekh, T. Anggara, A. Yezers, W.F. Schneider, J.T. Miller, W.N. Delgass, F.H. Ribeiro, *J. Catal.* 312 (2014) 87.
- [16] D.C. Calabro, J.C. Cheng, R.A. Crane, C.T. Kresge, S.S. Dhingra, M.A. Steckel, D.L. Stern, S.C. Weston, US Patent 6,049,018 (2000).
- [17] D.L. Dorset, S.C. Weston, S.S. Dhingra, *J. Phys. Chem. B* 110 (2006) 2045.
- [18] Ch. Baerlocher, L.B. McCusker, Database of Zeolite Structures, <http://www.iza-structure.org/databases/> (accessed 16.07.20).
- [19] G. Košová, *Stud. Surf. Sci. Catal.* 158A (2005) 59.
- [20] A. Chester, L.A. Green, S.S. Dhingra, T. Mason, H.K.C. Timken, US Patent 7,198,711 (2007).
- [21] T. Shibata, S. Suzuki, H. Kawagoe, K. Komura, Y. Kubota, Y. Sugi, J.-H. Kim, G. Seo, *Microporous Mesoporous Mat.* 116 (2008) 216.
- [22] Y. Kubota, S. Inagaki, Y. Nishita, K. Itabashi, Y. Tsuboi, T. Syahyah, T. Okubo, *Catal. Today* 243 (2015) 85.
- [23] S. Park, Y. Watanabe, Y. Nishita, T. Fukuoka, S. Inagaki, Y. Kubota, *J. Catal.* 319 (2014) 265.
- [24] A. Corma, V. Fornés, E. Palomares, *Appl. Catal. B* 11 (1997) 233.
- [25] J.G. Moscoso, D.Y. Jan, US Patent 7,922,997 (2011).
- [26] C.A. Emeis, *J. Catal.* 141 (1993) 347.
- [27] M.-F. Luo, P. Fang, M. He, Y.-L. Xie, *J. Mol. Catal. A* 239 (2005) 243.
- [28] Y. Kubota, K. Itabashi, S. Inagaki, Y. Nishita, R. Komatsu, Y. Tsuboi, S. Shinoda, T. Okubo, *Chem. Mater.* 26 (2014) 1250.
- [29] D. Jo, T. Ryu, G.T. Park, P.S. Kim, C.H. Kim, I.-S. Nam, S.B. Hong, *ACS Catal.* 6 (2016) 2443.
- [30] J.H. Kwak, D. Tran, J. Szanyi, C.H.F. Peden, J.H. Lee, *Catal. Lett.* 142 (2012) 295.
- [31] Y. Cheng, J. Hoard, C. Lambert, J.H. Kwak, C.H.F. Peden, *Catal. Today* 136 (2008) 34.
- [32] P.N.R. Vennestrøm, T.V.W. Janssens, A. Kustov, M. Grill, A. Puig-Molina, L.F. Lundsgaard, R.R. Tiruvalam, P. Concepción, A. Corma, *J. Catal.* 309 (2014) 477.
- [33] Y. Teraoka, C. Tai, H. Ogawa, H. Furukawa, S. Kagawa, *Appl. Catal. A* 200 (2000) 167.
- [34] M.C.N.A. de Carvalho, F.B. Passos, M. Schmal, *Appl. Catal. A* 193 (2000) 265.
- [35] M.H. Groothaert, K. Lievens, H. Leeman, B.M. Weckhuysen, R.A. Schoonheydt, *J. Catal.* 220 (2003) 500.
- [36] S.T. Korhonen, D.W. Fickel, R.F. Lobo, B.M. Weckhuysen, A.M. Beale, *Chem. Commun.* 47 (2011) 800.
- [37] J.H. Kwak, H. Zhu, J.H. Lee, C.H.F. Peden, J. Szanyi, *Chem. Commun.* 48 (2012) 4758.
- [38] R. Bulánek, B. Wichterlová, Z. Sobalík, J. Tichý, *Appl. Catal. B* 31 (2001) 13.
- [39] J.Y. Yan, G.D. Lei, W.M.H. Sachtler, H.H. Kung, *J. Catal.* 161 (1996) 43.
- [40] S. Contarini, L. Kevan, *J. Phys. Chem.* 90 (1986) 1630.
- [41] B.R. Strohmeier, D.E. Levden, R.S. Field, D.M. Hercules, *J. Catal.* 94 (1985) 514.
- [42] L. Pandolfi, P. Cafarelli, S. Kaciulis, A.A.G. Tomlinson, *Microporous Mesoporous Mat.* 110 (2008) 64.
- [43] N. Wilken, R. Nedyalova, K. Kamamasudram, J. Li, N. Currier, R. Vedaiyan, A. Yezers, L. Olsson, *Top. Catal.* 56 (2013) 317.
- [44] Y. Okamoto, K. Fukino, T. Imanaka, S. Teranishi, *J. Phys. Chem.* 87 (1983) 3740.
- [45] O.J. Durá, R. Boada, A. Rivera-Calzada, C. León, E. Bauer, M.A.L. de la Torre, J. Chaboy, *Phys. Rev. B* 83 (2011) 045202.
- [46] F. Göltl, R.E. Bulo, J. Hafner, P. Sautet, *J. Phys. Chem. Lett.* 4 (2013) 2244.
- [47] F. Gao, Y. Wang, N.M. Washton, M. Kollár, J. Szanyi, C.H.F. Peden, *ACS Catal.* 5 (2015) 678.